Multicomponent Space-Charge Transport Model for Ion-Exchange Membranes

Yahan Yang and Peter N. Pintauro
Dept. of Chemical Engineering, Tulane University, New Orleans, LA 70118

A multicomponent space-charge transport model for ion-exchange membranes was developed, where the membrane structure was modeled as an array of cylindrical pores with a uniform distribution of fixed-charge sites on the pore walls. Ion/fixed-charge site electrostatic interactions, electric-field-induced water dipole orientation, ion-hydration free-energy changes during ion partitioning, and concentration-dependent transport parameters were considered in the analysis. The model predicted experimental concentration vs. time data accurately for Donnan dialysis separations with a DuPont Nafion 117 cation-exchange membrane, where the membrane separated a dilute H_2SO_4 solution from an aqueous mixture of either $Cs_2SO_4 + Li_2SO_4$ or $Cs_2SO_4 + Na_2SO_4$. Both computer predictions and experimental measurements showed that the alkali metal cation with the larger hard-sphere radius (lower surface charge density) was selectively absorbed in and transported across the membrane during a multicomponent separation. The cation/cation transport permselectivity was less than the selectivity for equilibrium uptake due to slow ion transport near the pore wall, where discrimination between like-charge cations was greatest.

Introduction

The design of ion-exchange membranes can be greatly aided by ion and solvent structure/function transport models that contain (1) a mathematical description of the membrane microstructure; (2) relationships describing macroscopic (measurable) solute/solvent partitioning and the transport of ion species and water (solvent); and (3) fundamental theories relating the membrane structure to species fluxes and permselectivity, through molecular-level ion/solvent/polymer interactions. Such models can be used to propose new ion-exchange membranes with specific ion and solvent transport characteristics for a given electrochemical device (that is, a battery, fuel cell, and/or reactor) or separation process (that is, electrodialysis or Donnan dialysis). Additionally, a structure/function model could be used to simulate the performance of a given membrane in a particular electrochemical or separation application.

It is generally recognized that the overall permselectivity of salts by an ion-exchange membrane is governed by partitioning events at the upstream and downstream membrane/solution interfaces and transport through the interior of the membrane. Numerous theories have been proposed and tested to describe such sorption and transport events. One such ''space-charge'' model predefines the micro-level structure of an ion-exchange membrane as an array of pores (usually cylindrical) of known size with a specified distribution of ion-exchange sites on the pore walls. Model equations based on this structure include the Nernst-Planck and Navier-Stokes equations for the solute flux and solvent velocity, respectively. Electroneutrality in the pore fluid is not assumed and the Poisson-Boltzmann equation is used to calculate the radial-direction variations in electric potential and ion charge density. A nonzero space charge produces coupling between electrical forces, mass transfer, and fluid flow within the pore, which manifests itself in two ways: (a) the interaction of fluid flow and the electric field generates a body-force term in the momentum balance equation, and (b) the electrostatic potential in the space-charge region of the pore causes counterion enrichment and coion exclusion. Also, the interaction between the space-charge region and the driving forces for transport directed parallel to the pore wall results in such

Correspondence concerning this article should be addressed to P. N. Pintauro.
Present address of Y. Yang: Exxon Production Research Company, P. O. Box 2189, Houston, TX 77252.

electrokinetic phenomena as streaming potentials and electroosmosis. This modeling approach was first proposed by Osterle and coworkers nearly thirty years ago (Gross and Osterle, 1968; Fair and Osterle, 1971) and has since been used to describe electrokinetic effects in charged capillaries and ion-exchange membranes for single salts or salt/acid mixtures (see, for example, Sasidhar and Ruckenstein, 1982; Westermann-Clark and Anderson, 1983; Cwirko and Carbonell, 1989; Hijnen and Smit, 1995; Schmid, 1998; Kemery et al., 1998). None of these prior studies examined ion/solvent transport with a multicomponent salt solution on one side of the membrane.

The purpose of the work contained in this article was to develop and test a new capillary pore, space-charge structure/function transport model for multicomponent ion transport through an ion-exchange membrane. The model is a combination of the partition coefficient theory described by Pintauro and coworkers (Bontha and Pintauro, 1994; Pintauro et al., 1995), the single component space-charge transport model of Guzman-Garcia et al. (1990), and the electrokinetic membrane transport analysis of Gross and Osterle (1968). The present model considers several effects that are important during absorption and transport in highly charged membrane pores, specifically pore–water orientation by the strong radial-direction electric field generated by the membrane's fixed-charge sites (located on the membrane pore wall), variations in ion hydration forces within the membrane due to the low pore–water dielectric constant, and variations in pore–fluid viscosity due to the high concentration of counterions near the pore wall. For illustrative purposes, the model has been applied to the Donnan dialysis separation (Cwirko and Carbonell, 1990; Sato et al., 1991; Higa and Kira, 1992) of cations from an aqueous mixture of two alkali–metal sulfate salts, where a dilute aqueous salt mixture is separated from a sulfuric acid stripping solution by a commercial cation-exchange membrane. Protons are driven across the membrane and into the salt solution by the H^+ concentration gradient, whereas sulfate and bisulfate anions are effectively excluded from the membrane due to electrostatic repulsion forces. Because of its relatively large diffusivity, the diffusion flux of H^+ in the membrane will be larger than that of the back-diffusing monovalent cations. To maintain electroneutrality in both the salt and acid compartments, an electric field is established across the membrane to retard the movement of H^+ and facilitate the transport of one or both of the alkali metal cations. The electric field also generates a body force acting on the pore fluid, which gives rise to convective transport of water and ions. During a Donnan dialysis process, one can pump metal ions against their concentration gradients, so long as there is a transmembrane flux of H^+ and few mobile anions (coions) within the cation-exchange membrane (Lake and Melsheimer, 1978; Sudoh et al., 1987).

Theory

The theory for multicomponent ion and water transport in a cylindrical ion-exchange membrane pore begins with the definition of the electrochemical potential (μ) of each ion in the pore fluid. As was the case in previous membrane modeling studies (Guzman-Garcia et al., 1990; Babchin, 1993; Bontha and Pintauro, 1994), we define μ in terms of those nonidealities associated with ion–ion electrostatic interactions and ion hydration (solvation) effects:

$$\mu_i(x,r) = \mu_i^o + RT \ln C_i(x,r) + z_i F \Phi(x,r) + \Delta G_i, \quad (1)$$

where μ^o is the standard-state electrochemical potential, C is the ion concentration, Φ is the electric potential, z is the ion valence, ΔG is the hydration (solvation) Gibbs energy change associated with the transfer of an ion from vacuum to the pore fluid, and x and r are the axial and radial pore directions (where x is measured perpendicular to the membrane surface and does not include the pore tortuosity, and where $r = 0$ is the pore center line). The ΔG term in the preceding equation is replaced with $A_i/\epsilon(x,r)$ (Babchin, 1993; Bontha and Pintauro, 1994), where ϵ is the local solvent dielectric constant in a membrane pore, and A_i is an ion hydration constant, which is dependent on the hard-sphere ion radius, the solvent dipole moment and optical refractive index, and the bulk solvent dielectric constant.

The molar flux of each ion species (N_i) is defined in terms of its mobility (u_i), concentration, electrochemical potential gradient, and the pore fluid velocity, $v(x,r)$,

$$N_i(x,r) = -u_i C_i(x,r) \nabla \mu_i(x,r) + C_i(x,r) v(x,r). \quad (2)$$

The ion diffusion coefficient (D_i) is introduced into this equation by use of the Nernst-Einstein relationship ($u_i = D_i/RT$).

For a cylindrical membrane pore with $l/a \to \infty$ (where $l =$ the pore length and $a =$ the pore radius) and an impermeable pore wall, the radial ion fluxes and radial fluid velocity can be set equal to zero for all values of r (Westermann-Clark and Anderson, 1983; Sasidhar and Ruckenstein, 1982). Thus, there is an equilibrium distribution of ion species in the radial-pore direction and the axial-direction driving force for transmembrane ion movement will be the same at any radial pore position (Pintauro and Yang, 1995). Mathematically, one can write

$$\mu_i(x,r_1) = \mu_i(x,r_2) \quad (3)$$

or

$$\frac{d}{dx} u_i(x,r_1) = \frac{d}{dx} u_i(x,r_2) = \frac{d}{dx}\left[RT \ln C_i(x,0) + z_i F \Phi(x,0)\right]. \quad (4)$$

As indicated by Eq. 4, the $\nabla\mu$ driving-force terms in the ion-flux equations can be defined in terms of the concentration and electric potential gradient driving forces at the pore center line. There is no dielectric constant term on the right side of Eq. 4 because the centerline solvent dielectric constant is always equal to that in the bulk solution (that is, from symmetry arguments, there is no radial-direction electric field at the pore center line to preferentially align solvent dipoles).

As in previously published partition coefficient models for ion-exchange membranes (Bontha and Pintauro, 1994; Pintauro et al., 1995), a modified Boltzmann equation was used to describe the equilibrium distribution of ions in the radial

pore direction at any axial position,

$$C_i(x,r) = C_i(x,0)\exp\left[-\frac{z_i F[\Phi(x,r)-\Phi(x,0)]}{RT} - \frac{A_i}{RT}\left(\frac{1}{\epsilon(x,r)}-\frac{1}{\epsilon^b}\right)\right]. \quad (5)$$

It should be noted that Eq. 5 is consistent with our definition of electrochemical potential (Eq. 1), as discussed by Bontha and Pintauro (1994). In the preceding equation $\Phi(x,r)$ and $\epsilon(x,r)$ were computed by solving simultaneously Poisson's equation with a nonuniform dielectric constant and Booth's equation (Booth, 1951; Gur et al., 1978), which describes the decrease in solvent dielectric constant with increasing electric-field strength:

$$\nabla\cdot[\epsilon(x,r)\nabla\Phi(x,r)] = -\frac{F}{\epsilon^*}\sum_{i=1}^{n} z_i C_i(x,r) \quad (6)$$

$$\epsilon(x,r) = \zeta^2 + \frac{3(\epsilon^b-\zeta^2)}{\beta\nabla\Phi(x,r)}\left[\frac{1}{\tanh[\beta\nabla\Phi(x,r)]} - \frac{1}{\beta\nabla\Phi(x,r)}\right], \quad (7)$$

with

$$\beta = \left(\frac{5\alpha}{2\kappa T}\right)(\zeta^2+2). \quad (8)$$

In Eqs. 5–8, ϵ^b is the external (bulk) solution dielectric constant, ϵ^* is the permittivity of vacuum, κ is the Boltzmann's constant, ζ is the optical refractive index of the solvent, and α is the solvent dipole moment. Equation 7 is applicable for high electric fields ($\nabla\Phi > 2\times10^7$ V/m), which prior modeling studies have shown exist in the radial direction of highly charged membrane pores (Bontha and Pintauro, 1994; Pintauro et al., 1995).

The axial flux of mobile counterions and coions at a given axial position varies with radial position because of the radial-direction concentration profile (Eq. 5). The average flux of each ion species ($\overline{N}_i$) at a given value of x in a pore of radius a was computed from the following equation:

$$\overline{N}_i(x) \equiv \frac{\int_0^a N_i(x,r)2\pi r\,dr}{\pi a^2} = \frac{1}{\pi a^2}\int_0^a \times\left[-u_i\cdot\frac{d}{dx}\mu_i(x,r)\cdot C_i(x,r) + C_i(x,r)\cdot v(x,r)\right]2\pi r\,dr$$
$$= -\left[\frac{\int_0^a C_i(x,r)2\pi r\,dr}{\pi a^2}\right]\cdot\left\{u_i\frac{d}{dx}[RT\ln C_i(x,0) + z_i F\Phi(x,0)]\right\} + \frac{\int_0^a C_i(x,r)\cdot v(x,r)2\pi r\,dr}{\pi a^2}. \quad (9)$$

This equation is simply an integrated form of the well-known Nernst-Planck ion-flux equation, where the integration of the concentration is carried out to within one ion radius of the pore wall. The bracketed integral term in the second form of Eq. 9 is the radial-averaged concentration at a given axial pore position, and the second bracketed term is the concentration and electric potential-gradient driving-force expression at the pore center line, which is only a function of x. Such decoupling of the radial-direction concentration profile from the axial-direction driving force greatly simplifies the numerical solution of the model equations, especially when convective transport is small.

For the case of n mobile ion species in a membrane pore, the n ion flux equations (given by Eq. 9) are combined with $n-1$ steady-state conservation of species equations and one current density equation,

$$\frac{d}{dx}\overline{N}_i(x) = 0 \qquad i = 1,2,\ \ldots,\ n-1 \quad (10)$$

$$\sum_{i=1}^{n} z_i F\overline{N}_i(x) = J \quad (11)$$

where J is the current density, with units of A/cm^2.

The fluid velocity in a membrane pore is found by solving the continuity and steady-state Navier-Stokes equations (Fair and Osterle, 1971):

$$\nabla\cdot v(x,r) = 0$$
$$-\nabla P(x,r) + \eta\nabla^2 v(x,r) - \rho_e(x,r)\nabla\Phi(x,r) = 0, \quad (12)$$

where P is pressure, η is the pore fluid viscosity, and ρ_e is the charge density of mobile ions in the pore fluid,

$$\rho_e(x,r) = F\sum_{i=1}^{n} z_i C_i(x,r). \quad (13)$$

Equations 12 and 13 have been incorporated into previous space-charge membrane transport models (Westermann-Clark and Anderson, 1980; Guzman-Garcia et al., 1990) and their use is based on an assumed continuum/constant-density model for water in a membrane pore.

Transient changes in salt concentration in the bulk solution reservoirs on either side of the membrane were found by introducing mass-balance equations for each reservoir (Cwirko and Carbonell, 1989), which are of the form

$$\frac{d[V\cdot C_i^b]}{dt} = \frac{s\theta\overline{N}_i}{\tau} \qquad \text{with} \qquad \frac{d[V]}{dt} = \frac{s\theta v^\dagger}{\tau}, \quad (14)$$

where V is the reservoir volume (assumed to be initially the same on either side of the membrane), s is the total membrane area, θ is the membrane porosity, τ is the pore tortuosity, and $v^\dagger$ is the pore-averaged axial fluid velocity. The use of Eq. 10 in a membrane pore and Eq. 14 in the external reservoirs is based on the assumption that membrane fluxes are at quasi-steady-state, that is, the time constant for transport in the membrane is much shorter than the time scale characterizing observable ion concentration changes in the

two well-mixed solution reservoirs adjacent to the membrane. It is also assumed that there is sufficient stirring in the reservoirs to eliminate mass-transfer resistance by liquid boundary-layers on either side of the membrane.

Boundary conditions for the transport model in the radial-pore direction for all values of x are (1) symmetry in electric potential and a zero radial fluid velocity at the pore center line, and (2) Gauss' law, the no-slip hydrodynamic condition, and an impenetrable pore wall at $r = a$ (where a is the pore radius):

$$\text{at } r = 0, \qquad \frac{\partial \Phi}{\partial r} = 0; \quad \epsilon = \epsilon^b; \quad v_r = 0 \tag{15}$$

$$\text{at } r = a, \qquad \frac{d\Phi}{dr} = -\frac{\sigma}{\epsilon^* \epsilon(a)}; \quad v_x = 0; \quad v_r = 0. \tag{16}$$

Boundary conditions in the axial pore direction are (1) the pressure in the membrane pore at the pore entrance ($x = 0$) and exit ($x = L$, where L is the membrane thickness), which is related to the osmotic pressures of the reservoir solutions,

$$P(x,r) = P^o + RT\left(\sum_{i=1}^{n} C_i(x,r) - C_i^b\right) \qquad \text{for} \quad x = 0 \quad \text{and} \quad x = L, \tag{17}$$

where P^o is atmospheric pressure (the two reservoirs on either side of the membrane are vented to the atmosphere); and (2) the radial-direction concentration, electric potential, and dielectric constant profiles at the membrane pore/reservoir inlet and exit. These profiles, which quantify the process of equilibrium ion partitioning at $x = 0$ and $x = L$, are determined using a previously published partition coefficient model consisting of Eqs. 6–8 and a modified form of Eq. 5, where the bulk external concentration of species i replaces $C_i(x,0)$ and Φ^b (the electric potential in the external solution) replaces the centerline potential (Bontha and Pintauro, 1994);

$$C_i(x,r) = C_i^b \exp\left\{\frac{-z_i F\left[\Phi(x,r) - \Phi^b\right]}{RT} - \frac{A_i}{RT}\left(\frac{1}{\epsilon(x,r)} - \frac{1}{\epsilon^b}\right)\right\}. \tag{18}$$

In the computational scheme, Φ^b was arbitrarily set equal to zero in one reservoir (to fix the zero ground state potential) and Φ^b was calculated by the model for the second reservoir.

The theory was tested for the Donnan dialysis separation of aqueous mixtures of two alkali metal sulfate salts (either $Cs_2SO_4 + Li_2SO_4$ or $Cs_2SO_4 + Na_2SO_4$) with a sulfuric acid receiving solution and a Nafion 117 cation-exchange membrane (Nafion is a registered trademark of E. I. DuPont de Nemours and Co., Inc.). The initial concentrations on the salt and acid sides of the membrane for these experiments are listed in Table 1. Model equations were written for the transport of water, cations, and all bisulfate anions (HSO_4^- and MSO_4^-, where M refers to an alkali-metal species) and were solved numerically using standard finite difference techniques. Although $SO_4^=$ can exist in the solutions outside the membrane, sulfonate salts within the membrane pores are not fully dissociated (Verbrugge and Hill, 1988, 1990; Guzman-Garcia et al., 1990). The aim of the present study was to evaluate the model's capability of predicting competitive cation (counterion) transport, hence the salt and acid concentrations were set well below the ion-exchange capacity of the Nafion membrane (0.909 mmol/g) in order to minimize coion (anion) intrusion and transport. Donnan dialysis is a zero net current transport process because electroneutrality must be maintained in the two compartments that are separated by the membrane; thus, the current density in Eq. 11 was equal to zero.

Table 1. Initial Salt and Acid Concentrations for the Donnan Dialysis Experiments

	Salt Solution	Acid Solution
Exp. No. 1	0.125 M Li_2SO_4 + 0.125 M Cs_2SO_4	0.25 M H_2SO_4
Exp. No. 2	0.125 M Na_2SO_4 + 0.125 M Cs_2SO_4	0.25 M H_2SO_4
Exp. No. 3	0.125 M Li_2SO_4 + 0.0054 M Cs_2SO_4	0.125 M H_2SO_4

Determination of model parameters

The transport theory contains a number of membrane structure, ion hydration, and solute and solvent transport parameters that must be specified before a membrane separation process can be simulated. Microstructure parameters (pore radius, a, and pore wall charge density, σ) for the Nafion 117 membrane used in the present study were estimated from equilibrium membrane swelling experiments and small-angle X-ray scattering data in the literature, according to the following equations (Guzman-Garcia et al., 1990):

$$a = a_w\left[\frac{s}{s_w}\frac{\theta}{\theta_w}\right]^{1/2} \tag{19}$$

$$\sigma = \frac{\rho_{\text{dry}}(1-\theta)(\text{IEC})aF}{2\theta}, \tag{20}$$

where a, s, and θ are the pore radius, membrane sample area, and membrane porosity after equilibration in a salt/acid solution and s_w, a_w, and θ_w, are the corresponding quantities for the same membrane equilibrated in water. The dry density of Nafion 117 (ρ_{dry}) was set equal to 1.84×10^3 kg/m^3, and its ion-exchange capacity (IEC) was 0.909 mmol/g. From small-angle X-ray scattering data in the literature, a_w was set at 2.75 nm (Gierke et al., 1981). The porosity of a Nafion membrane was determined from changes in the dry and wet membrane volumes,

$$\theta = \frac{\text{VOL}_{\text{wet}} - \text{VOL}_{\text{dry}}}{\text{VOL}_{\text{wet}}}. \tag{21}$$

Single, time-invariant values of the pore radius, pore wall charge density, and membrane porosity were used when modeling transport during a Donnan dialysis experiment. Such data were collected with a Nafion 117 film that was equilibrated in a salt/acid aqueous mixture with a concentra-

Table 2. Pore Radius, Pore Wall Charge Density, and Porosity of Nafion 117 Membranes for the Equilibrium Uptake and Donnan Dialysis Simulations

	Salt/Acid Solution Composition	Pore Radius (nm)	Pore Wall Charge Density (C/m^2)	Membrane Porosity
Equilibrium Uptake*	$H^+ + Li^+$	2.56	0.42	0.37
	$H^+ + Na^+$	2.38	0.46	0.33
	$H^+ + K^+$	1.99	0.57	0.25
	$H^+ + Cs^+$	1.90	0.64	0.23
Donnan Dialysis**				
Exp. No. 1	0.0625 M Li_2SO_4 0.0624 M Cs_2SO_4 0.125 M H_2SO_4	1.96	0.59	0.24
Exp. No. 2	0.0625 M Na_2SO_4 0.0625 M Cs_2SO_4 0.125 M H_2SO_4	1.96	0.59	0.24
Exp. No. 3	0.0625 M Na_2SO_4 0.0027 M Cs_2SO_4 0.0625 M H_2SO_4	2.31	0.48	0.48

*Solutions were 0.125 M H_2SO_4 + 0.125 M M_2SO_4 (where M = Li, Na, K, or Cs).
**See Table 1 for the initial salt concentrations during Donnan dialysis Exps. 1–3.

tion equal to that present in the dialysis cell reservoirs at the end of a Donnan dialysis experiment (when the system is at equilibrium and all transport ends). The membrane structure data for the computer simulation codes of the Donnan dialysis experiments in Table 1 are listed in Table 2. The membrane pore tortuosity in Eq. 14 could not be determined from an independent experimental measurement and was considered an adjustable parameter in the model.

Cation and anion hydration parameters, A_i, in the modified Boltzmann equation (Eqs. 5 and 18) were calculated using the following relationship (Bontha and Pintauro, 1994):

$$A_i = \frac{(\Delta G_i)_{\text{hyd}}^{\zeta^2} - (\Delta G_i)_{\text{hyd}}^{b}}{\frac{1}{\zeta^2} - \frac{1}{\epsilon^b}}. \qquad (22)$$

Data in the literature (Halliwell and Newberg, 1963; Rosseinsky, 1965) were used for $\Delta G_{\text{hyd}}^{b}$, the Gibbs energy of ion hydration in the bulk electrolyte (where the dielectric constant is ϵ^b). $\Delta G_{\text{hyd}}^{\zeta 2}$, the Gibbs hydration energy in a fluid of dielectric constant ζ^2 (where ζ is the optical refractive index of the solvent), was calculated from the following equation (Bontha and Pintauro, 1994):

$$(\Delta G_i)_{\text{hyd}}^{\zeta^2} = -\frac{\mathbb{N} z_i^2 e^2}{8\pi\epsilon^* \mathbb{R}_i} + \frac{\mathbb{N} z_i^2 e^2}{8\pi\epsilon^* \mathbb{R}_i \zeta^2}, \qquad (23)$$

where $\mathbb{N}$ is Avogadro's number, e is the charge on an electron, and $\mathbb{R}_i$ is the hard-sphere ion radius. Values of A_i for the various alkali metal cations and the bisulfate anion used in the Donnan dialysis experiments are listed in Table 3. $\Delta G_{\text{hyd}}^{b}$ for H^+ was not available in the literature due to the uncertainty in the radius of a proton in water (that is, it is not known whether the proton exits in the H^+ or H_3O^+ form). To circumvent this problem, A_{H+} was determined by force fitting the ion uptake model (Eqs. 6–8 and 18) to experimental data for the equilibrium absorption of aqueous alkali metal cation/H^+ mixtures into a Nafion 117 membrane (as will be discussed in detail in the following section).

For the transport parameters in the model, we chose to use infinite-dilution cation and anion diffusion coefficients (where the diffusivities of HSO_4^- and MSO_4^- were set equal) and electric mobilities that were corrected for the concentration of ions in the Nafion pore. It has been shown in previous equilibrium ion uptake models with a Nafion 117 membrane that there is strong attraction of counterions to the pore-wall fixed charges, with a very high concentration of cations near the pore wall (Bontha and Pintauro, 1994). To account for this effect, the infinite dilution diffusion coefficients, D^o (listed in Table 3), and mobilities, u^o (calculated from D^o by the Nernst-Einstein relationship), were modified using a concentration-dependent solvent viscosity,

$$D_i(r) = \frac{D_i^o \eta^o}{\eta(r)} \qquad \text{and} \qquad u_i(r) = \frac{D_i(r)}{RT}, \qquad (24)$$

where $\eta(r)$ is given by the Einstein viscosity equation (Hiemenz, 1977; Smedley, 1980), which was written in terms of the infinite-dilution solvent viscosity (η^o) and the local solute (anion + cation) volume fraction (λ),

$$\eta(r) = \eta^0 \frac{1 + \lambda(r)/2}{[1 - \lambda(r)]^2}, \qquad (25)$$

where

$$\lambda(r) = \sum_i C_i(r) \mathbb{N} \left(\frac{4}{3} \pi \mathbb{R}_i^3 \right) \times 10^{-3}. \qquad (26)$$

Experimental

Equilibrium uptake experiments for the determination of A_{H+}

An initial set of equilibrium uptake experiments was performed with a Nafion 117 cation-exchange membrane and aqueous mixtures of 0.125 M H_2SO_4 plus 0.125 M M_2SO_4 (where M = Li, Na, K, and Cs) at 25°C, in order to determine the hydration parameter (A_i) for H^+. Standard procedures of membrane pretreatment, soaking, leaching, and drying were used to determine the equilibrium concentrations of metal cations and H^+ in Nafion membrane samples (see, for example, Bontha and Pintauro, 1994).

A computer optimization program searched systematically for a single value of A_{H+} that produced the best fit of computed and experimentally measured ion/proton uptake selectivities, S_{H+}^{M+}. Experimentally, the selectivity was determined using the following equation:

$$S_{H^+}^{M^+} = \frac{C_{H^+}^{b}}{C_{H^+}^{m}} \times \frac{C_{M^+}^{m}}{C_{M^+}^{b}}, \qquad (27)$$

where C_{M+}^{m} and C_{H+}^{m} are the measured concentrations of metal cations and H^+ inside the membrane, respectively.

Table 3. Hard-Sphere Radius,* Hydration Constant, and Infinite Dilution Diffusivity of Cations and Bisulfate Anion**

	R_i (nm)	A_i (J/mol)	D_i^o (cm^2/s)
H^+	* * *	* * *	9.31×10^{-5}
Li^+	0.078	2.23×10^5	1.03×10^{-5}
Na^+	0.102	2.09×10^5	1.33×10^{-5}
Cs^+	0.169	1.92×10^5	2.06×10^{-5}
HSO_4^-	0.193	2.31×10^5	1.33×10^{-5}

*Goldschmidt (1927) ion radius.
**From Newman (1991).

Theoretically, $S_{H^+}{}^{M^+}$ was found by integrating (up to one ion radius from the pore wall) the computed radial-direction ion concentration profiles in a Nafion 117 pore:

$$S_{H^+}{}^{M^+} = \frac{C^b_{H^+}}{\int_0^a C_{H^+}(x, r)2\pi r\, dr} \times \frac{\int_0^a C_{M^+}(x, r)2\pi r\, dr}{C^b_{M^+}}. \quad (28)$$

Experimentally determined pore radii, pore wall densities of fixed-charge sites, and membrane porosities for the different aqueous salt/acid mixtures used in the uptake experiments are listed in Table 2. The match of experimental and theoretical selectivities with a single, optimized value of A_{H+} (261,071 J/mol) is shown in Figure 1, where $S_{H+}{}^{M+}$ is plotted vs. the alkali metal cation hydration parameter (A_{M+}).

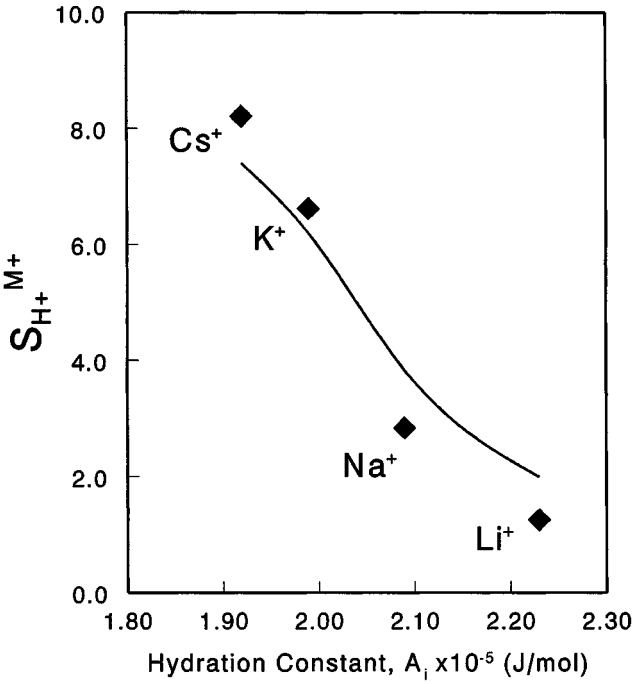

Figure 1. Computer predictions and experimental measurements of selectivities for alkali metal cation uptake with respect to H^+ for a Nafion 117 membrane equilibrated in a solution containing sulfuric acid (0.125 M) and an alkali metal sulfate salt (0.125 M).

◆ Experimental data; —— model calculations.

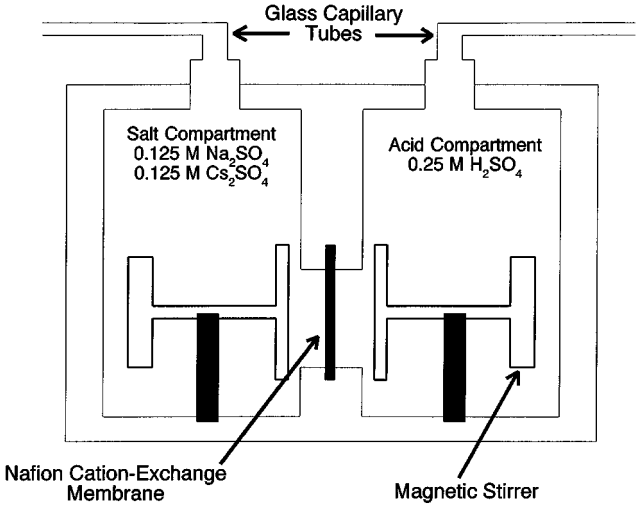

Figure 2. Donnan dialysis cell.

The agreement of the uptake model and experimental data is good, especially for the larger alkali metal cations (Cs^+, K^+, and Na^+) where the discrepancy between the model and measurements is $\approx 9\%$. As would be expected based on our previous studies (Bontha and Pintauro, 1994), the theoretical and experimental M^+/H^+ selectivities increase with decreasing A_{M+} (increasing hard sphere ion radius) because (1) the dielectric constant of water near the pore wall was reduced significantly by the strong electric field generated by the membranes' pore-wall fixed-charge sites, and (2) the solubility of metal cations in the low dielectric constant pore-wall region is inversely proportional to the ion's surface-charge density.

Multicomponent Donnan dialysis experiments

Donnan dialysis experiments were carried out at a constant temperature of 25°C using the cell shown in Figure 2. A Nafion membrane (5.1-cm^2 area) separated two compartments, each with a volume of 285 mL, containing sampling ports (open to the atmosphere) and Teflon-coated magnetic stirrers. One of the cell chambers was filled initially with a dilute H_2SO_4 solution and the other chamber contained an aqueous mixture of two alkali metal sulfate salts (the initial acid and salt mixture concentrations for these experiments are listed in Table 1). The concentrations of protons and cation species in each cell compartment were determined periodically over 72 h (the time required for equilibration of the salt and acid solutions) by withdrawing 0.5-mL solution samples and analyzing each sample for H^+ (by titration with NaOH) and metal cations (by flame atomic absorption spectrophotometry using a Perkin-Elmer Model 5000 spectrometer). The same experiments were repeated to measure water flow across the membrane, where a horizontally positioned precision-bore glass capillary tube (3 mm ID and partially filled with fluid) was connected to each compartment's sampling port. Changes in solution volume in the reservoirs on either side of the membrane, due to fluid flow across the membrane, were monitored over the course of each Donnan dialysis experiment by tracking the fluid position in each capillary tube.

Results and Discussion

Solution viscosity effects and the prediction of cation permselectivity

Our first task was to evaluate the applicability of Eqs. 24–26 (for the concentration-dependent viscosity, ion diffusivity, and electric mobility) in the membrane transport model, using reservoir concentration vs. time data from Donnan dialysis experiment #1 (Table 1), where a Nafion membrane separated initially solutions of 0.125 M Li_2SO_4 + 0.125 M Cs_2SO_4 from 0.250 M H_2SO_4. Theoretical and experimental results are shown in Figure 3 as the Cs^+/Li^+ concentration ratio in the acid compartment vs. the Li^+ concentration in the acid compartment. In such a plot, the model calculations are independent of pore tortuosity (an as yet undetermined parameter in the model). From the material balance equations for the reservoirs in contact with the membrane (Eq. 14), we can combine mathematically the membrane tortuosity and real time, t, in which case it can be inferred that $C_i^{b,\mathrm{I}}$ and $C_i^{b,\mathrm{II}}$ scale linearly with the inverse of the tortuosity (where the superscripts I and II refer to the bulk solution reservoirs). Since $C_i^{b,\mathrm{I}} = C_i^{b,\mathrm{I}}(t/\tau)$ and $C_i^{b,\mathrm{II}} = C_i^{b,\mathrm{II}}(t/\tau)$ (that is, since tortuosity is simply a scaling factor for real time), a plot of $C_1^{b,\mathrm{II}}/C_2^{b,\mathrm{II}}$ vs. $C_1^{b,\mathrm{II}}$ or $C_2^{b,\mathrm{II}}$ will be independent of τ. Thus, the results in Figure 3 provide an unambiguous test of both the transport model (with no fitting parameters) and the use of the concentration-corrected transport parameters. For comparison purposes, model predictions are also shown for the case of no viscosity corrections and for a pore-solution viscosity given by the Lyklema-Overbeek equation (Lyklema and Overbeek, 1961), which relates the increase in $\eta(r)$ to the electric-field strength, $E(r)$, in a membrane pore [where $E(r) \equiv -\nabla\Phi(r)$],

$$\eta(r) = \eta^0\left[1 + 10.2\times10^{-16}E(r)^2\right]. \qquad (29)$$

As can be seen in Figure 3, there is excellent agreement between the experimental measurements and model predictions when the Einstein equation was used to correct the pore-fluid viscosity and the infinite dilution ion diffusivities and mobilities. The computed Cs^+/Li^+ concentration ratio (the membrane cation transport selectivity) was overestimated by the model when there was no concentration dependence on η, D^o, and u^o, and the pore fluid viscosity was too high near the wall and the predicted ion selectivities were too low when the Lyklema-Overbeek equation was incorporated into the model. As a consequence of this analysis, Eqs. 24–26 were used for all subsequent transport model computations.

The results in Figure 3 also provide important insights into the mechanism of multicomponent cation transport in a cation-exchange membrane. It has been shown previously by Bontha and Pintauro (1994) that the computed radial-direction concentration profiles for two different monovalent cations in a Nafion 117 membrane pore under equilibrium sorption conditions differ substantially in the vicinity of the pore wall ($r/a > 0.9$), where the electric field (generated by the membrane fixed charges) is high, water dipoles are aligned [$\epsilon(r) \ll \epsilon^b$, in accordance with Eq. 7], and unfavorable hydration forces suppress the concentration of the monovalent cation with the smaller hard-sphere radius (that is, the cation

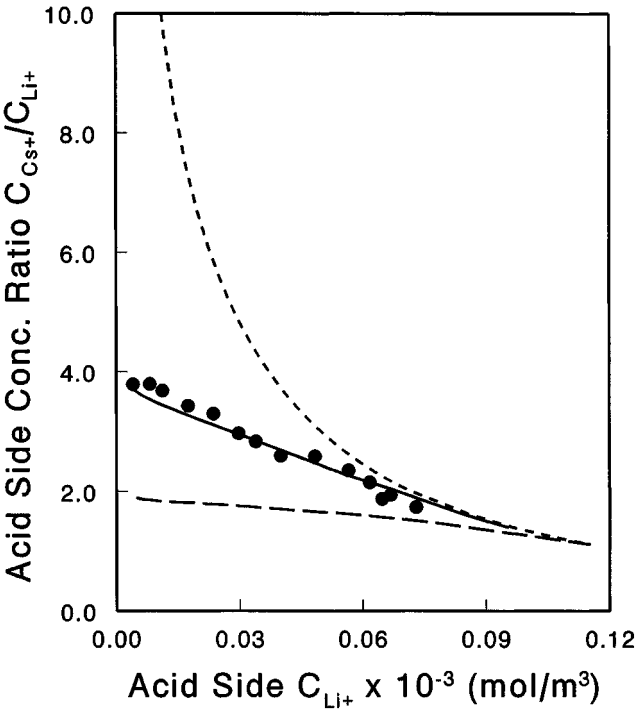

Figure 3. Cs^+/Li^+ permselectivity results from a Donnan dialysis experiment with a Nafion 117 membrane and initial concentrations of 0.25 M H_2SO_4 and 0.125 M Li_2SO_4 + 0.125 M Cs_2SO_4.

● Experimental data; —— Model simulation with the Einstein viscosity equation; – – – Model simulation with no viscosity corrections; ———— Model simulation with the Lyklema-Overbeek viscosity equation (a = 1.96 nm, σ = 0.59 C/m^2, θ = 0.24).

with the higher surface-charge density and larger value of A_i). A similar concentration difference exists at the pore/salt–solution interface during multicomponent Donnan dialysis, as shown in Figures 4a and 4b, where the initial $C_{Cs+}(r)$, $C_{Li+}(r)$, and $C_{H+}(r)$ profiles are plotted at the Nafion pore entrance and exit. These profiles are dependent on the sum of electrostatic attraction energies and repulsive energies associated with the Gibbs energy of ion hydration (see Eq. 7). The local maximum in the counterion-concentration profiles at $r/a \approx 0.8$ is associated with the radial location where the dielectric constant decreases dramatically (Bontha and Pintauro, 1994). Although the equilibrium absorption selectivity for Cs^+ and Li^+ (S_{Li+}^{Cs+}, according to Eq. 28) based on the results in Figure 4a was large (≈ 12), the Cs^+/Li^+ transport selectivity in Figure 3 was initially low (≈ 4) because the solution viscosity near the pore wall was high (the total counterion concentration increases rapidly as $r \to a$), which suppressed ion movement where C_{Cs+} and C_{Li+} differed most. This point is illustrated in Figure 3, where the computed Cs^+/Li^+ concentration ratio in the acid chamber of the Donnan dialysis cell during the initial stages of the Donnan dialysis separation was > 10 for the case where $\eta(r) = \eta^o$, $D_i(r) = D_i^o$ and $u_i(r) = u_i^o$ (that is, when ion transport near the pore wall was uninhibited by viscosity effects).

Thus, we can conclude that the high solution viscosity near the pore wall, due to the high concentration of cation (coun-

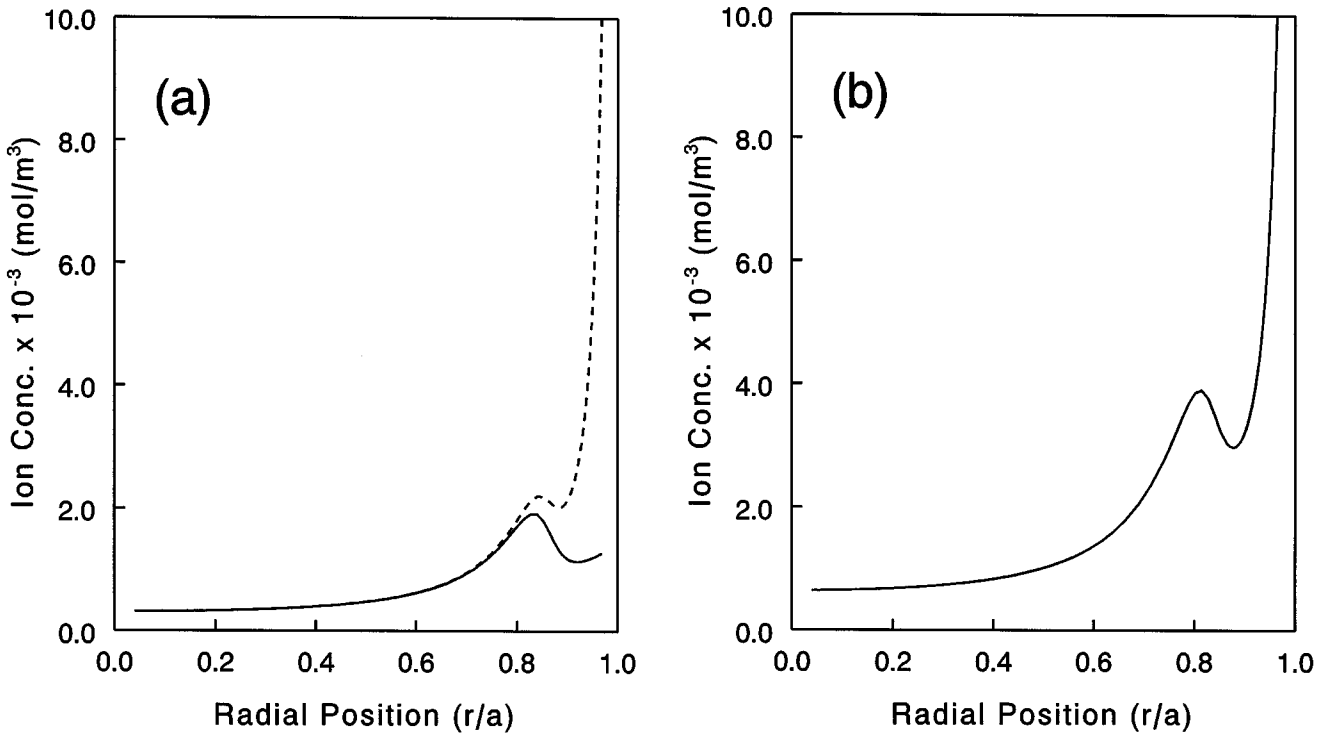

Figure 4. Initial radial concentration profiles for counterions at the pore entrance and exit for the Donnan dialysis experiment with Nafion 117 and initial concentrations of 0.25 M H_2SO_4 and 0.125 M Li_2SO_4 + 0.125 M Cs_2SO_4.

(a) – – – Cs^+ at the pore/salt solution interface; —— Li^+ at the pore/salt solution interface; (b) H^+ at the pore/acid solution interface.

terion) species, effectively limits cation/cation permselectivity during transport, as compared to that observed during equilibrium absorption. This point was tested further by performing transport model calculations with three hypothetical values of the membrane fixed-charge density ($\sigma = 0.2$, 0.4, and 0.59 C/m^2) and a constant pore radius of 1.96 nm, where the initial salt and acid solutions for Donnan dialysis were identical to those in Figure 3. Based on Eqs. 5–8, one would expect greater cation/cation uptake discrimination by the membrane at the pore entrance with increasing pore-wall fixed-charge concentration, but the results in Figure 5 show an upper bound in Cs^+/Li^+ selectivity with increasing wall charge. For $\sigma > 0.4$ C/m^2, the benefit of having greater differentiation in the radial-direction concentration profiles of Cs^+ and Li^+ (that is, higher cation/cation sorption selectivity) is counterbalanced by the higher concentration of counterions near the pore wall, which causes the fluid viscosity to increase and the transport rates of ions in the pore wall region (where $C_{Cs+} \gg C_{Li+}$) to decrease. It should also be noted that there is essentially no variation in pore-solvent dielectric constant and no significant cation/cation absorption selectivity (only transport selectivity based on differences in cation diffusivities) when the pore-wall charge density is less than about 0.1 C/m^2 (for a 1.96-nm radius pore).

Returning to Figure 3, we see that viscosity effects in the pore wall region no longer influenced ion transport during the later stages of the multicomponent batch Donnan dialysis experiment as indicated by the merging of all three model curves. The Cs^+/Li^+ selectivity also decreased as the Donnan dialysis experiment progresses (that is, as the Li^+ concentration in the acid compartment increases). We have attributed these findings to decreases in the axial-direction electric field and ion-concentration gradient driving forces near the pore wall. Whereas the Cs^+, Li^+, and H^+ concentrations near the pore center line are of the same magnitude as the external salt/acid solutions and mimic the rise and fall of salt/acid outside the membrane, the counterion concentrations near the pore wall are controlled by the membrane's fixed charges [that is, even when $C_i(0, x)$ is small, the counterion concentrations as $r \rightarrow a$ will be high in accordance with the modified Boltzmann equation and the Gauss' law boundary condition]. As Cs^+, Li^+, and H^+ penetrated through the pore during the initial stages of a Donnan dialysis experiment, the radial-direction electric potential and ion-concentration profiles near the pore wall at all axial positions became almost identical (even at the pore exit, adjacent to the acid chamber, Cs^+ and Li^+ replaced H^+ near the pore wall, as indicated by the selectivity results in Figure 1). We can conclude that as a batch Donnan dialysis separation progresses, ion transport in the center region of the pore dominates where (1) the ion concentrations are not particularly high (so that the concentration or electric-field corrections to η^o are small and the different viscosity models in Figure 3 give the same result), and (2) the difference in Cs^+ and Li^+ concentrations is small, which causes the observed and predicted cation/cation transport selectivities in Figure 3 to de-

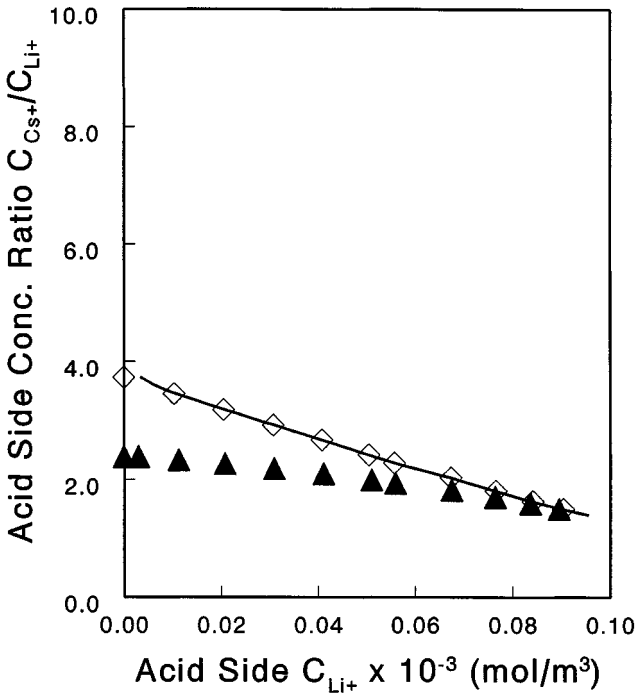

Figure 5. Effect of pore wall charge density on computed Cs^+/Li^+ permselectivity for a Donnan dialysis experiment with Nafion 117 and initial concentrations of 0.25 M H_2SO_4 and 0.125 M Li_2SO_4 + 0.125 M Cs_2SO_4.

▲ $\sigma = 0.20$ C/m^2; ◇ $\sigma = 0.40$ C/m^2; —— $\sigma = 0.59$ C/m^2 ($a = 1.96$ nm, $\theta = 0.24$).

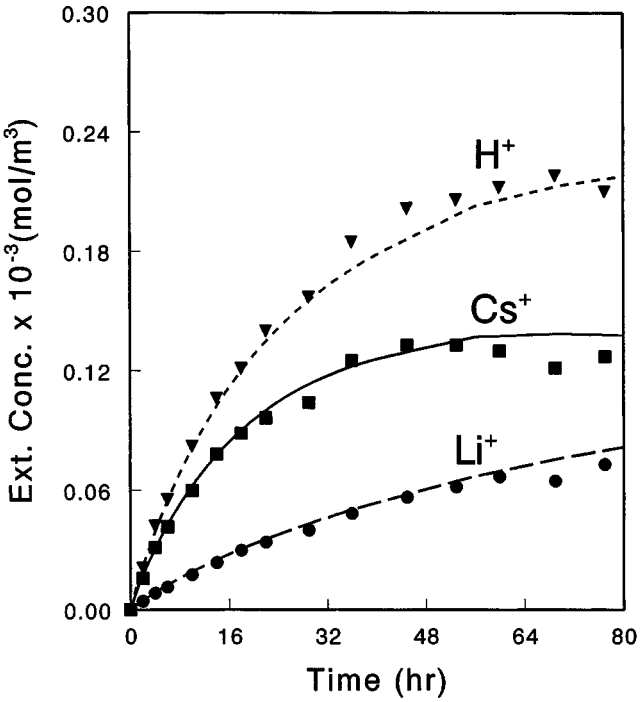

Figure 6. Measured and computed external proton and cation concentrations in the salt and acid chambers of the Donnan dialysis cell, respectively.

Nafion 117 membrane and initial solutions of 0.25 M H_2SO_4 and 0.125 M Li_2SO_4 + 0.125 M Cs_2SO_4. Symbols are experimental data points (■ Cs^+; ● Li^+; ▼ H^+), and lines are model predictions ($a = 1.96$ nm, $\sigma = 0.59$ C/m^2, $\theta = 0.24$, $\tau = 8.0$).

crease. We can further infer from this analysis that a decrease in membrane counterion/counterion permselectivity will accompany the well-known decrease in ion fluxes, as a multicomponent batch Donnan dialysis separation proceeds to its equilibrium (zero flux) state.

Multicomponent ion transport during Donnan dialysis

The pore tortuosity, which appears in Eq. 14, must be specified if the model were to predict concentration vs. time data in the two reservoirs of the Donnan dialysis cell. In the present analysis the tortuosity was treated as an adjustable parameter, as was the case in previous studies (see, for example, Sasidhar and Ruckenstein, 1982), and a single, time-invariant value of τ was found for each Donnan dialysis experiment by matching the model predictions to the initial five experimental data points for metal cation and proton concentrations (taken over a period of about 2 h). This tortuosity was then used to compute proton and alkali metal cation concentration changes over the 16–20 h course of an entire Donnan dialysis experiment.

The transient Li^+ and Cs^+ concentrations in the acid compartment of the Donnan dialysis cell and the H^+ concentration variations in the salt compartment are shown in Figure 6 for the 0.125 M Li_2SO_4 + 0.125 M Cs_2SO_4 and 0.25 M H_2SO_4 system (Experiment No. 1 in Table 1). With a constant tortuosity of 8.0, the match of the computer simulation with concentration measurements is excellent for the entire experiment, with discrepancies $< 7\%$. Both the experimental data and model calculations show that Cs^+ has a higher flux than Li^+ and approaches equilibrium faster than Li^+ when they are both present in and transported simultaneously across the Nafion 117 membrane. A computer simulation of a 0.125 M Na_2SO_4 + 0.125 M Cs_2SO_4 and 0.25 M H_2SO_4 Donnan dialysis experiment (Experiment #2 in Table 1) was also performed, as shown in Figure 7. Again, the tortuosity was determined from the first five concentration measurements for Cs^+ and Na^+ in the acid compartment and H^+ concentration in the salt compartment (resulting in $\tau = 7.5$). Again, we see that Cs^+ was transported selectively through the membrane to the acid compartment in this multicomponent Donnan dialysis experiment. Because the equilibrium uptake selectivity between cesium and sodium is smaller than that of a $Cs^+ + Li^+$ mixture (Bontha and Pintauro, 1994) and because of the smaller difference between the Cs^+ and Na^+ diffusion coefficients, as compared to that between Cs^+ and Li^+ (see Table 3), the Cs^+/Na^+ transport selectivity throughout the experiment in Figure 7 was smaller than that between Cs^+ and Li^+ in Figure 6.

A comparison of the various ion-flux components for the lithium/cesium/proton Donnan dialysis simulation provided information as to the mode of transport for the individual ion species. After appropriate substitution, the ion molar flux

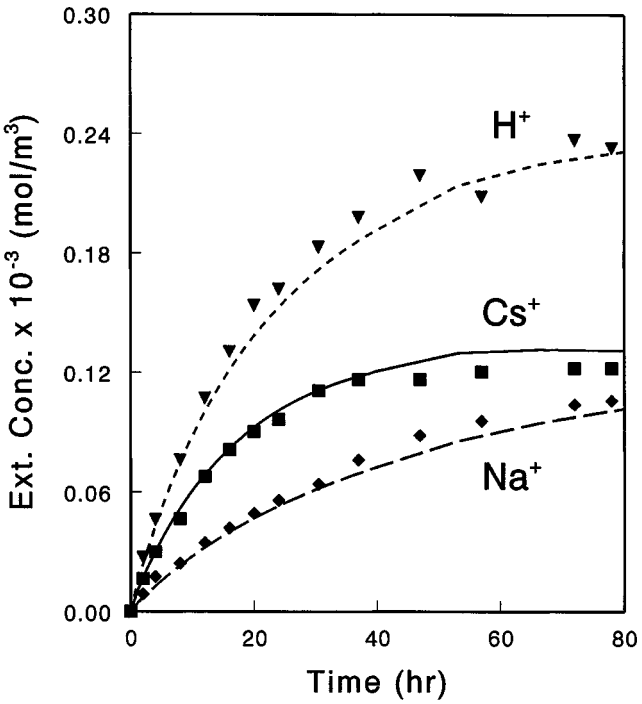

Figure 7. Measured and computed external proton and cation concentrations in the salt and acid chambers of the Donnan dialysis cell, respectively.

Nafion 117 membrane and initial solutions of 0.25 M H_2SO_4 and 0.125 M Na_2SO_4 + 0.125 M Cs_2SO_4. Symbols are experimental data points (■ Cs^+; ◆ Na^+; ▼ H^+), and lines are model predictions ($a = 1.96$ nm, $\sigma = 0.59$ C/m^2, $\theta = 0.24$, $\tau = 7.5$).

equation (Eq. 2) can be decomposed into diffusion, migration, convection, and hydration components:

$$N_{i,\,\mathrm{diff}}(x,\,r) = -\,D_i \frac{d}{dx} C_i(x,\,r) \tag{30}$$

$$N_{i,\,\mathrm{mig}}(x,\,r) = -\,D_i C_i(x,r) \frac{z_i F}{RT} \frac{d}{dx} \Phi(x,\,r) \tag{31}$$

$$N_{i,\,\mathrm{hyd}}(x,\,r) = -\,D_i C_i(r,x) \frac{A_i}{RT} \frac{d}{dx}\left(\frac{1}{\epsilon(x,r)}\right) \tag{32}$$

$$N_{i,\,\mathrm{con}}(x,r) = C_i(x,\,r)\upsilon(x,\,r). \tag{33}$$

Even though the integrated total flux for each ion species is independent of the membrane axial-pore position due to mass conservation, the individual flux components are, by definition, functions of axial and radial pore locations. Mathematically, N_{diff}, N_{mig}, N_{conv}, and N_{hyd} change with x because the axial ion-concentration profiles deviate from linear straight lines, which would be the case for pure diffusion (Yang, 1999). To facilitate our analysis, the overall pore-averaged flux component for an ion species was defined as follows,

$$N_{i,\mathrm{comp}}^{\mathrm{av}} = \frac{\left(2\int_0^L \int_0^a N_{i,\,\mathrm{comp}}(x,\,r)\,r\,dr\,dx\right)}{a^2 L} \times \frac{\theta}{\tau}, \tag{34}$$

where the subscript *comp* refers to the individual flux components: diffusion, migration, convection, and hydration. Results of $N_{j,\mathrm{diff}}^{av}$, $N_{j,\mathrm{mig}}^{\mathrm{av}}$, $N_{j,\mathrm{conv}}^{\mathrm{av}}$, and $N_{j,\mathrm{hyd}}^{\mathrm{av}}$ as a function of time for Cs^+, Na^+, and H^+, are shown in Figures 8a–8c for the Donnan dialysis experiment with an initial salt mixture of 0.125 M Na_2SO_4 and 0.125 M Cs_2SO_4 (at $x = 0$) and an initial acid solution of 0.25 M H_2SO_4 (at $x = L$). As expected, the diffusion and migration components are the major contributors to the counterion fluxes. For H^+, the electric field in the axial-pore direction acts to slow down diffusion, and thus the sign of the migration flux is opposite that due to diffusion. Because of the relatively high concentration of mobile cesium ions inside the pore (that is, the high absorption selectivity for Cs^+) and because the migration flux is directly proportional to the mobile ion concentration and the axial gradient in the electric field, the migration flux for cesium dominates over its diffusional component, whereas the diffusion flux component for Li^+ is largest because the concentration of lithium ions inside the membrane pore is small. The diffusion flux for cesium becomes negative before the system reaches equilibrium because Cs^+ has a higher uptake selectivity in the acid compartment vs. H^+ than it has in the salt compartment vs. Li^+, resulting in more Cs^+ inside the membrane at the membrane/acid interface than at the membrane/salt solution interface (this only occurred after a significant amount of Cs^+ had accumulated in the acid chamber). The convective flux component for all three cations was small compared to the diffusion and migration terms, due to a low water velocity near the pore wall where the majority of counterions are present. Because ion movement by convection occurs primarily in the region away from the pore wall where there is no selectivity in ion concentration, the convective fluxes for the different cations are nearly equal. Thus, it can be concluded that convection is at best a nonfactor and at worst may lower cation/cation permselectivity during Donnan dialysis (when the total salt and acid concentrations are initially equal). The hydration flux component for all cations is negative (movement in the direction of the salt chamber) due to the driving force associated with variations in the water dielectric constant. Since it is more difficult for H^+ to approach closely the membrane pore wall as compared to an alkali metal cation (due to the larger value of A_{H+}), the electric field in the radial-pore direction at the membrane/acid interface is stronger than that at the membrane/salt solution interface. According to the Booth equation (Eq. 7), a larger electric field produces a smaller value for $\epsilon(x,r)$, hence the axial-direction derivative of $1/\epsilon(x,r)$ is < 0 in the interior of the pore for $r \neq 0$. Although not shown here, the model-computed bisulfate anion fluxes that were two orders of magnitude lower than the proton and mobile cation transport rates (Yang, 1999), as expected for a cation-exchange membrane with external salt-solution concentrations that were much lower than the membrane ion-exchange capacity.

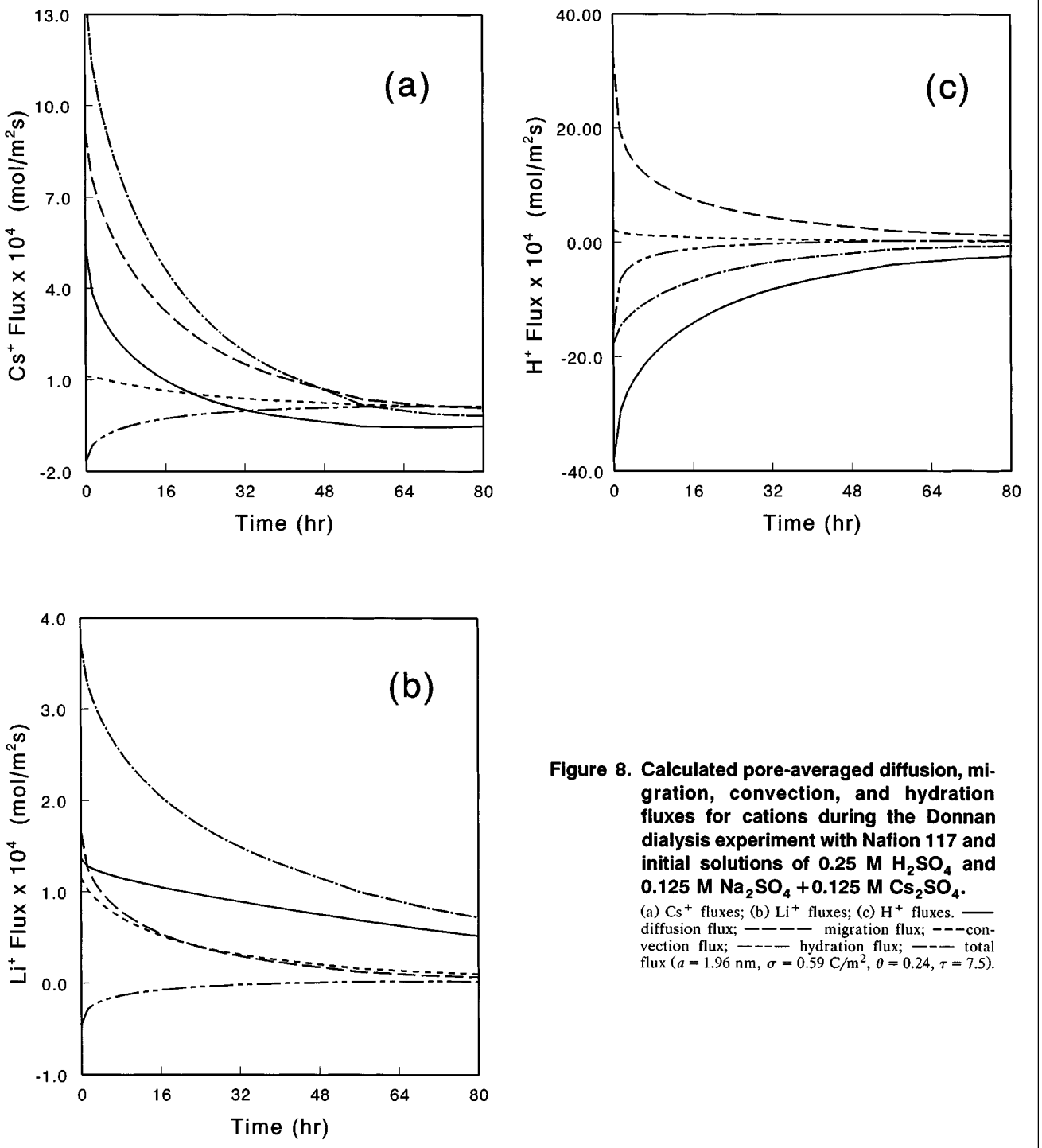

Figure 8. Calculated pore-averaged diffusion, migration, convection, and hydration fluxes for cations during the Donnan dialysis experiment with Nafion 117 and initial solutions of 0.25 M H_2SO_4 and 0.125 M Na_2SO_4 + 0.125 M Cs_2SO_4.

(a) Cs^+ fluxes; (b) Li^+ fluxes; (c) H^+ fluxes. —— diffusion flux; ———— migration flux; - - - convection flux; ———— hydration flux; ——— total flux (a = 1.96 nm, σ = 0.59 C/m^2, θ = 0.24, τ = 7.5).

The computed axial-direction voltage difference across a Nafion pore, defined as Φ^b(acid chamber) − Φ^b(salt chamber), is plotted against time in Figure 9 for the Cs_2SO_4/Li_2SO_4 Donnan dialysis experiment. The higher electric potential in the salt compartment of the cell gave rise to an electric-field driving force that actively transported Cs^+ and Li^+ from the salt reservoir into the acid compartment and slowed the back-transport of protons into the salt reservoir. The potential also generated a small electroosmotic water flux in the direction of the acid compartment. As expected, the transmembrane voltage difference decreased as the solutions on either side of the membrane equalized with time.

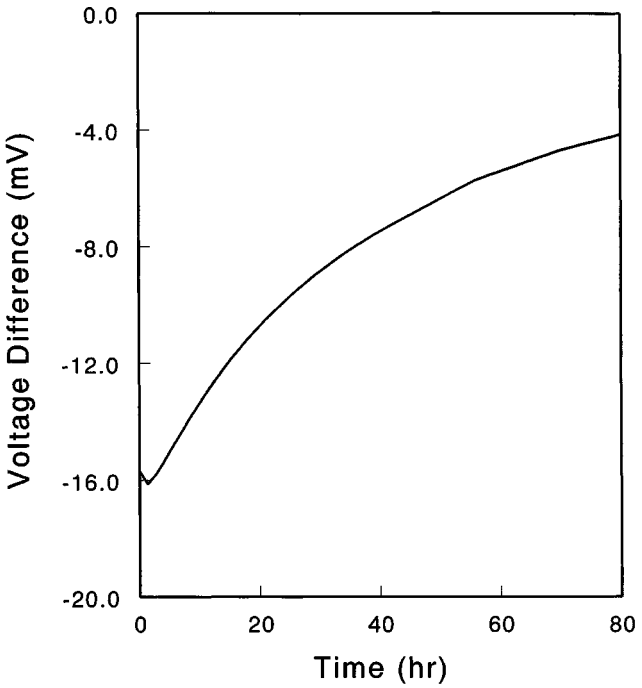

Figure 9. Computed electric potential difference across a Nafion 117 membrane (potential in the acid chamber–potential in the salt chamber) during a Donnan dialysis experiment with initial solutions of 0.25 M H_2SO_4 and 0.125 M Li_2SO_4 + 0.125 M Cs_2SO_4.

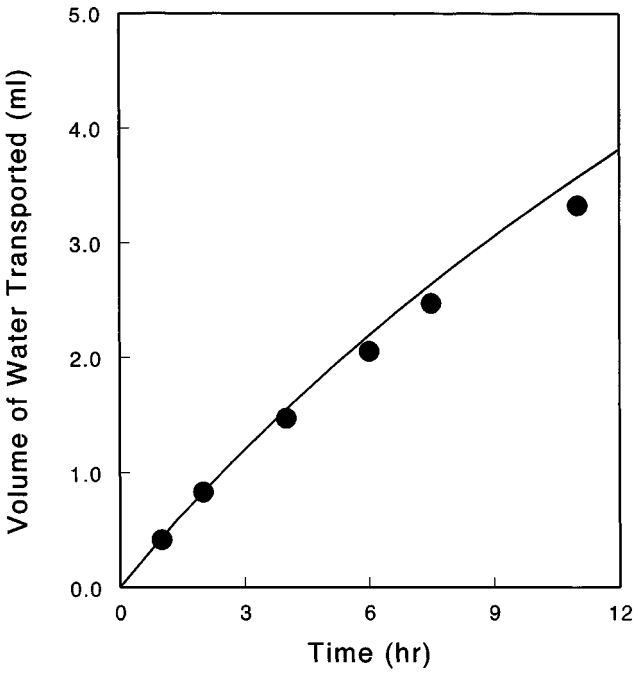

Figure 10. Computed and measured water transport rates (from the salt to the acid chamber) during the Donnan dialysis experiment with Nafion 117 and initial solutions of 0.25 M H_2SO_4 and 0.125 M Na_2SO_4 + 0.125 M Cs_2SO_4.

● Experimental; —— model calculations.

Water transport during multicomponent Donnan dialysis

To illustrate the model's ability to predict the transmembrane water flux, computed and measured changes in the acid reservoir volume with time are shown in Figure 10 for Donnan dialysis experiment No. 2 (cf. Table 1), where a 0.25 M H_2SO_4 solution was separated initially from a mixture of 0.125 M Na_2SO_4 and 0.125 M Cs_2SO_4. As expected, the water flux was small due to a modest electroosmotic driving force and the absence of an osmotic pressure difference across the membrane (because the total concentration of ions in the salt and acid compartments was the same initially and the flux of coions through Nafion was small). The electric potential body force acting on the pore water is proportional to $\rho_e \times \nabla\Phi$ (see Eq. 12) and was large in the pore-wall region where the counterion concentration was high, but viscosity effects diminished the fluid velocity near the pore wall. Since the vast majority of ions within the Nafion membrane were positively charged (because the external salt concentration was much less than the membrane fixed-charge concentration), the direction of the electroosmotic force acting on the pore fluid was in the same direction as the electric field, and thus the flow of pore water occurred from the salt compartment to the acid reservoir. Computed water velocity profiles at various times for the Na^+/Cs^+ Donnan dialysis experiment are shown in Figure 11. The profiles are parabolic-like in shape, but differ substantially from a Poiseuille velocity profile and are not the same as those from a previous space-charge membrane transport model (Guzman-Garcia et al., 1990) that did not consider a concentration-dependent pore fluid viscosity.

Case of a concentration gradient reversal

The voltage drop across an ion-exchange membrane during Donnan dialysis is generated to maintain electroneutrality for all ions in the external reservoirs. Thus, the voltage difference and the resulting ion-migration fluxes are dependent on the external bulk salt concentrations of all ions present in each reservoir, as opposed to the diffusion flux, which is calculated from the concentration gradient of a single ion species. An interesting concentration dynamic behavior has been observed for one multicomponent Donnan dialysis experiment (Experiment No. 3 in Table 1) because of this complex dependence of transmembrane voltage drop on the external ion concentrations. In Figure 12, experimental and theoretical concentration data for this Donnan dialysis separation are shown. The experimental dialysis conditions were similar to those in Figure 7, except that the initial cesium ion concentration in the salt compartment was greatly reduced. In contrast to the metal cation and proton curves in Figure 7, here it was found that the cesium-ion concentration in the acid compartment increased with time and overshot its equilibrium value. The computer model gave correct predictions for both the appearance of the peak value in the Cs^+ profile and the relative magnitude of the concentration overshoot. The unexpected cesium behavior was due to the low concentration of Cs^+ in the membrane pore and the high voltage difference across the membrane that was necessary to maintain electroneutrality because of the large difference between the proton and sodium ion diffusivities (see Table 3). Conse-

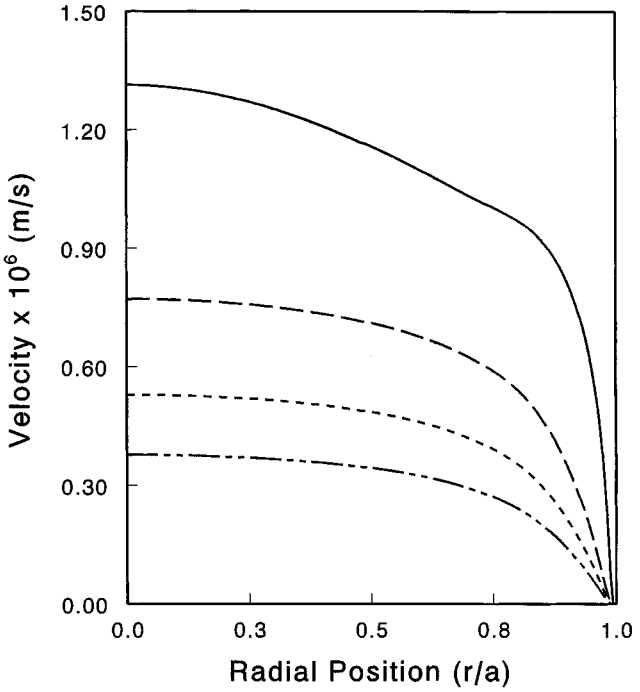

Figure 11. Computed radial-direction water-velocity profiles within a Nafion 117 pore during a Donnan dialysis experiment with initial solutions of 0.25 M H_2SO_4 and 0.125 M Na_2SO_4 +0.125 M Cs_2SO_4.

—— $t = 0$; ———— $t = 11$ h; ----- $t = 24$ h; ———— $t = 37$ h.

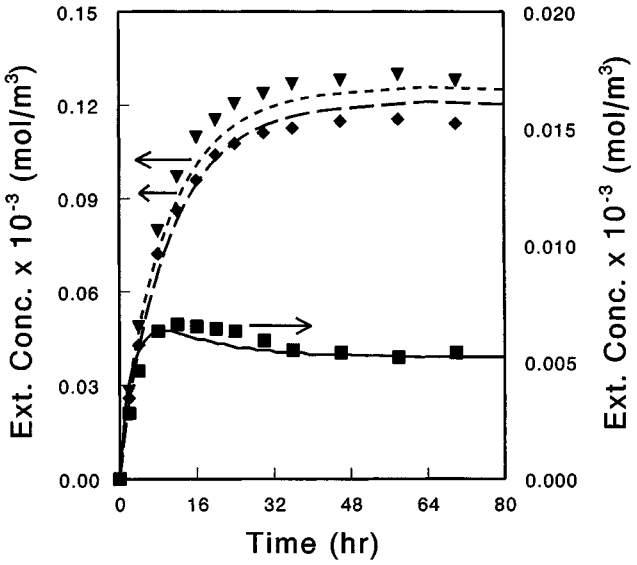

Figure 12. Measured and computed proton and cation concentrations in the salt and acid chambers of the Donnan dialysis cell, respectively.

Nafion 117 membrane and initial solutions of 0.125 M H_2SO_4 and 0.125 M Na_2SO_4 + 0.0054 M Cs_2SO_4. Symbols are experimental data points (■ Cs^+; ◆ Na^+; ▼ H^+), and lines are model predictions ($a = 1.96$ nm, $\sigma = 0.59$ C/m^2, $\theta = 0.24$, $\tau = 7.5$).

quently, the migration component of the cesium flux, which dominated over its diffusion component, quickly brought the cesium-ion concentration in the acid compartment to a level close to that in the salt compartment. Although the diffusional flux component for cesium quickly approached zero, the diffusion of Na^+ and H^+ persisted and the transmembrane voltage continued to drive Cs^+ from the salt compartment to the acid compartment, against its concentration gradient. As the system approached its final equilibrium state, the voltage difference across the membrane decreased to zero and Cs^+ back-diffused from the acid compartment to the salt compartment due to the reversal in its concentration gradient.

Conclusions

A multicomponent space-charge transport model for an ion-exchange membrane containing highly charged pores has been developed and applied to the batch Donnan dialysis separation of alkali metal cation salts. The membrane microstructure was defined as an array of cylindrical pores of known radius with a uniform distribution of ion-exchange sites on the pore walls. The model took into account ion/fixed-charge electrostatic interactions, water dipole orientation due to the strong electric field generated by the membrane's fixed-charge groups, ion-hydration free-energy changes that occur during ion partitioning, and concentration-dependent transport properties. The Einstein viscosity equation was used to relate pore fluid viscosity to solute concentration and to correct infinite dilution ion diffusivities and mobilities for concentration effects. Electric potential, solvent dielectric constant, water velocity, and cation and anion concentration profiles in the radial and axial pore directions were computed by solving numerically Poisson's equation containing a modified Boltzmann equation, Booth's equation, the Navier-Stokes equations, and the Nernst-Planck equations.

The model predicted accurately experimental concentration vs. time data for Donnan dialysis separations with a Nafion 117 cation-exchange membrane, where the membrane separated a dilute (0.25 M) H_2SO_4 solution from an aqueous mixture of either $Cs_2SO_4 + Li_2SO_4$ or $Cs_2SO_4 + Na_2SO_4$. Both computer predictions and experimental measurements showed that the alkali metal cation with the larger hard-sphere radius was selectively absorbed in and transported across the membrane in the multicomponent separation system. The model also simulated accurately the flux of water across the membrane during multicomponent Donnan dialysis.

From the match of model calculations with macroscopic concentration changes across the membrane during a Donnan dialysis experiment and from the computed radial-direction concentration profiles (which were assumed to be correct although they could not be measured experimentally), we have arrived at a number of conclusions regarding the mechanism of cation/cation separation in a Nafion film. The cation/cation (such as Cs^+/Li^+) transport selectivity of Nafion during Donnan dialysis was lower than that observed during equilibrium membrane sorption experiments with an alkali metal cation salt mixture, due to the high solution vis-

cosity and the resulting low ion transport rates near the pore-wall, where the difference in concentration of the two cations was greatest. Increasing the membrane's pore-wall charge density will increase the cation/cation absorption selectivity, but will not necessarily improve separation performance due to a decrease in the cation fluxes (higher cation concentrations and solution viscosity) near the pore wall. Also, a decrease in membrane cation/cation permselectivity accompanied the decreases in ion fluxes as a multicomponent batch Donnan dialysis experiment proceeded to its equilibrium (zero flux) state, due to a rapid decrease in the axial direction driving forces near the pore wall.

Acknowledgments

This work was supported by the National Science Foundation Grant No. EHR-9108765.

Literature Cited

Babchin, A. J., "Modified Nernst-Planck Equation for Hydration Effects," *J. Colloid Interface Sci.*, **160**, 258 (1993).

Bontha, J. R., and P. N. Pintauro, "Water Orientation and Ion Solvation Effects During Multicomponent Salt Partitioning in a Nafion Cation Exchange Membrane," *Chem. Eng. Sci.*, **49**, 3835 (1994).

Booth, F. J., "The Dielectric Constant of Water and Saturation Effect," *J. Chem. Phys.*, **19**, 391 (1951).

Cwirko, E. H., and R. G. Carbonell, "Transport of Electrolytes in Charged Pores: Analysis Using the Method of Spatial Averaging," *J. Colloid Interface Sci.*, **129**, 513 (1989).

Cwirko, E. H., and R. G. Carbonell, "A Theoretical Analysis of Donnan Dialysis Across Charged Porous Membranes," *J. Memb. Sci.*, **48**, 155 (1990).

Fair, J. C., and F. F. Osterle, "Reverse Electrodialysis in Charged Capillary Membranes," *J. Phys. Chem.*, **54**, 3307 (1971).

Gierke, T. D., G. E. Munn, and F. C. Wilson, "The Morphology in Nafion Perfluorinated Membrane Products, as Determined by Wide- and Small-Angle X-Ray Studies," *J. Poly. Sci.*, **19**, 1687 (1981).

Goldschmidt, N. M., "Krystallban und Chemische Zusammensetzung," *Chem. Ber.*, **60**, 1263 (1927).

Gross, R. J., and J. F. Osterle, "Membrane Transport Characteristics of Ultrafine Capillaries," *J. Phys. Chem.*, **49**, 228 (1968).

Gur, Y., I. Ravina, and A. J. Babchin, "On the Electric Double Layer Theory. II. The Poisson-Boltzmann Equation Including Hydration Forces," *J. Colloid Interface. Sci.*, **64**, 333 (1978).

Guzman-Garcia, A. G., P. N. Pintauro, M. W. Verbrugge, and R. F. Hill, "Development of a Space-Charge Transport Model for Ion-Exchange Membranes," *AIChE J.*, **36**, 1061 (1990).

Halliwell, H. F., and S. C. Newberg, "Enthalpy of Hydration of the Proton," *Trans. Faraday Soc.*, **59**, 1126 (1963).

Hiemenz, P. C., *Principles of Colloid and Surface Chemistry*, Dekker, New York (1977).

Higa, M., and A. Kira, "Theory and Simulation of Ion Transport in Nonstationary States Against Concentration Gradients Across Ion-exchange Membranes," *J. Phys. Chem.*, **96**, 9518 (1992).

Hijnen, H. J. M., and J. A. M. Smit, "Effect of the pH on Electrolyte Transport Through Microporous Membranes Bearing Either Weakly or Strongly Dissociated Acid Groups. A Theoretical Analysis Using the Space-Charge Model for a Cylindrical Capillary," *J. Memb. Sci.*, **99**, 285 (1995).

Kemery, P. J., J. K. Steehler, and P. W. Bohn, "Electric Field Mediated Transport in Nanometer Diameter Channels," *Langmuir*, **14**, 2884 (1998).

Lake, M. A., and S. S. Melsheimer, "Mass Transfer Characterization of Donnan Dialysis," *AIChE J.*, **24**, 130 (1978).

Lyklema, J., and J. Th. G. Overbeek, "On the Interpretation of Electrokinetic Potentials," *J. Colloid Interface Sci.*, **16**, 501 (1961).

Newman, J. S., *Electrochemical Systems*, 2nd ed., Prentice Hall, Englewood Cliffs, NJ (1991).

Pintauro, P. N., R. Tandon, L. Chao, W. Xu, and R. Evilia, "Equilibrium Partitioning of Monovalent/Divalent Cation-Salt Mixtures in Nafion Cation-Exchange Membranes," *J. Phys. Chem.*, **99**, 12915 (1995).

Pintauro, P. N., and Y. Yang, "Structure/Function Modeling: A Rational Approach to Ion-Exchange Membrane Design," *Electrochem. Soc. Proc.*, **95-11**, The Electrochemical Society, Pennington, NJ (1995).

Rossiensky, D., "Electrode Potentials and Hydration Energies: Theories and Correlations," *Chem. Rev.*, **65**, 467 (1965).

Sasidhar, V., and E. Ruckenstein, "Anomalous Effects During Electrolyte Osmosis Across Charged Porous Membranes," *J. Colloid Interface Sci.*, **85**, 332 (1982).

Sato, K., C. Fukuhara, T. Yonemoto, and T. Tadaki, "Ionic Transport in a Continuous Donnan Dialyzer with a Parallel Plate Channel and an Agitated Tank," *J. Chem. Eng. Jpn.*, **24**, 81 (1991).

Schmid, G., "Electrochemistry of Capillary Systems with Narrow Pores. I. Overview," *J. Membr. Sci.*, **150**, 151 (1998).

Smedley, S. I., "The Interpretation of Ionic Conductivity in Liquids, Plenum, New York (1980).

Sudoh, M., H. Kamei, and S. Nakamura, "Donnan Dialysis Concentration of Cupric Ions," *J. Chem. Eng. Jpn.*, **20**, 34 (1987).

Verbrugge, N. W., and R. F. Hill, "Experimental and Theoretical Investigation of Perfluorosulfonic Acid Membranes Equilibrated with Aqueous Sulfuric Acid Solutions," *J. Phys. Chem.*, **92**, 6778 (1988).

Verbrugge, M. W., and R. F. Hill, "Ion and Solvent Transport in Ion-Exchange Membranes II. A Radiotracer Study of the Sulfuric-Acid, Nafion 117 System," *J. Electrochem. Soc.*, **137**, 893 (1990).

Westerman-Clark, G. B., and J. L. Anderson, "Experimental Verification of the Space Charge Model for Electrokinetics in Charged Capillary Pores," *J. Electrochem. Soc.*, **130**, 839 (1983).

Yang, Y., "Electrostatic Interactions and Electrokinetic Transport in Ion-exchange Membranes," PhD Diss., Tulane Univ., New Orleans, LA (1999).

Manuscript received Aug. 2, 1999, and revision received Jan. 3, 2000.